

# GAN-BASED MULTIPLE ADJACENT BRAIN MRI SLICE RECONSTRUCTION FOR UNSUPERVISED ALZHEIMER'S DISEASE DIAGNOSIS

Changhee Han<sup>(1,2)</sup>, Leonardo Rundo<sup>(3,4)</sup>, Kohei Murao<sup>(1)</sup>, Zoltán Ádám Milacski<sup>(5)</sup>,  
Kazuki Umemoto<sup>(6)</sup>, Hideki Nakayama<sup>(2)</sup>, Shin'ichi Satoh<sup>(1)</sup>

(1) Research Center for Medical Big Data, National Institute of Informatics, Tokyo, Japan,  
han@nlab.ci.i.u-tokyo.ac.jp

(2) Graduate School of Information Science and Technology, The University of Tokyo, Tokyo, Japan

(3) Department of Radiology, University of Cambridge, Cambridge, United Kingdom

(4) Cancer Research UK Cambridge Centre, Cambridge, United Kingdom

(5) Department of Artificial Intelligence, ELTE Eötvös Loránd University, Budapest, Hungary

(6) Department of Rehabilitation Medicine, Juntendo University School of Medicine, Tokyo, Japan

*Keywords:* Generative adversarial networks, Alzheimer's disease diagnosis, Unsupervised anomaly detection, Brain MRI reconstruction.

**Abstract.** Leveraging large-scale healthy datasets, unsupervised learning can discover various unseen diseases without any annotation. Towards this, unsupervised methods reconstruct a single medical image to detect outliers either in the learned feature space or from high reconstruction loss. However, without considering continuity between multiple adjacent images, they cannot directly discriminate diseases composed of the accumulation of subtle anatomical anomalies, such as Alzheimer's Disease (AD). Moreover, no study shows how unsupervised anomaly detection is associated with disease stages. Therefore, we propose a two-step method using Generative Adversarial Network-based multiple adjacent brain MRI slice reconstruction to detect AD at various stages: (*Reconstruction*) Wasserstein loss with Gradient Penalty +  $\ell_1$  loss—trained on 3 healthy brain MRI slices to reconstruct the next 3 ones—reconstructs unseen healthy/AD cases; (*Diagnosis*) Average/Maximum loss (e.g.,  $\ell_2$  loss) per scan discriminates them, comparing the reconstructed/ground truth images. The results show that we can reliably detect AD at a very early stage (i.e., Area Under the Curve (AUC) 0.780) while also detecting AD at a late stage (i.e., AUC 0.917) much more accurately; since our method is unsupervised, it should also discover and alert any anomalies including rare disease.

## 1 Scientific Background

Deep Learning can achieve accurate computer-assisted diagnosis when large-scale annotated training samples are available [1]. In medical imaging, unfortunately, preparing such massive annotated datasets is often impossible; to tackle this, researchers have proposed various data augmentation techniques, including Generative Adversarial Network (GAN)-based ones [2, 3, 4]. However, even exploiting these techniques, supervised learning still requires many pathological images, even for rare disease, to conduct reliable diagnosis; nevertheless, it can only detect already-learned specific pathologies. In this regard, as physicians detect unseen anomalies using prior information on healthy body structure, unsupervised anomaly detection methods leveraging only large-scale healthy images can discover and alert unseen disease when their generalization fails.

Towards this, researchers reconstructed a single medical image *via* GANs [5], AutoEncoders (AEs) [6, 7], or combining them [8], since GANs can generate realistic images and AEs, especially Variational AEs [9], can directly map data onto its latent representation;

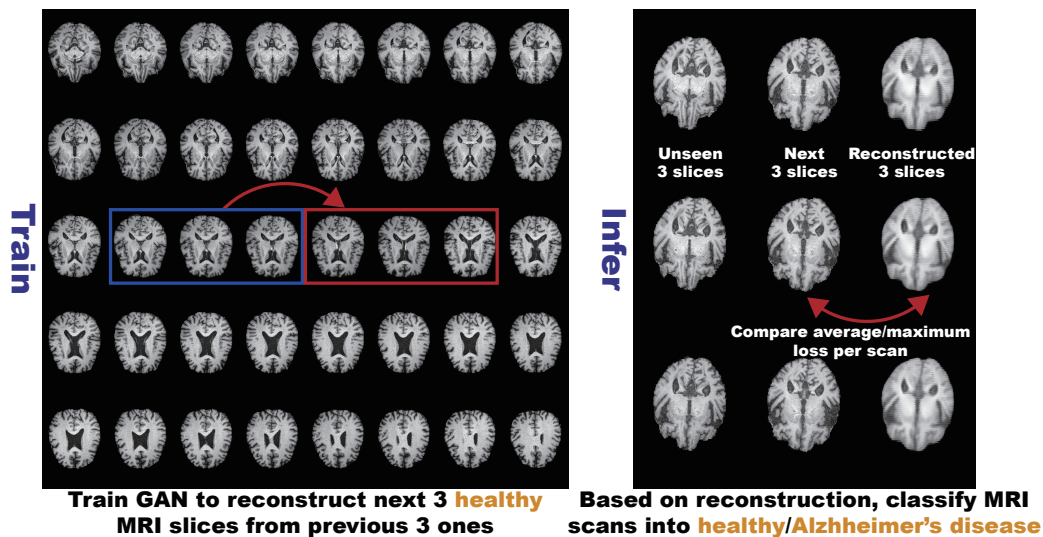


Figure 1: Unsupervised AD diagnosis framework: We train WGAN-GP +  $\ell_1$  loss on 3 healthy brain axial MRI slices to reconstruct the next 3 ones, and test it on both unseen healthy and AD cases to classify them based on average/maximum loss (e.g.,  $\ell_2$  loss) per scan.

then, unseen images were scored by comparing them with reconstructed ones to discriminate a pathological image distribution (i.e., outliers either in the learned feature space or from high reconstruction loss). However, those single image reconstruction methods mainly target diseases easy-to-detect from a single image even for non-expert humans, such as glioblastomas on Magnetic Resonance (MR) images [10] and lung cancers on Computed Tomography images [11]. Without considering continuity between multiple adjacent images, they cannot directly discriminate diseases composed of the accumulation of subtle anatomical anomalies, such as Alzheimer’s Disease (AD). Moreover, no study shows how unsupervised anomaly detection is associated with disease stages.

Therefore, we propose a two-step method using GAN-based multiple adjacent brain MRI slice reconstruction to detect AD at various stages (Fig. 1): (*Reconstruction*) Wasserstein loss with Gradient Penalty (WGAN-GP) [12] +  $\ell_1$  loss—trained on 3 healthy brain axial MRI slices to reconstruct the next 3 ones—reconstructs unseen healthy/AD cases; (*Diagnosis*) Average/Maximum loss (e.g.,  $\ell_2$  loss) per scan discriminates them, comparing the reconstructed/ground truth images. Using 1, 133 healthy MRI scans for training, our approach can reliably detect AD at a very early stage (i.e., Area Under the Curve (AUC) 0.780) while also detecting AD at a late stage (i.e., AUC 0.917) much more accurately—implying its ability to also detect any other diseases.

**Contributions.** Our main contributions are as follows:

- **MRI Slice Reconstruction:** This first multiple MRI slice reconstruction approach can predict the next 3 brain MRI slices from the previous 3 ones only for unseen images similar to training data by combining WGAN-GP and  $\ell_1$  loss.
- **Unsupervised Anomaly Detection:** This first unsupervised anomaly detection across different disease stages reveals that, like physicians’ way of diagnosis, massive healthy data can reliably aid early diagnosis, such as of MCI, while also detecting late-stage disease much more accurately by discriminating with  $\ell_2$  loss.
- **Alzheimer’s Disease Diagnosis:** This first unsupervised AD diagnosis study can reliably detect AD and also any other diseases.

## 2 Materials and Methods

### 2.1 OASIS-3 Dataset

We use a longitudinal dataset of  $176 \times 240/176 \times 256$  T1-weighted (T1w) 3T brain axial MRI slices containing both normal aging subjects/AD patients extracted from the Open Access Series of Imaging Studies-3 (OASIS-3) [13]. The  $176 \times 240$  slices are zero-padded to reach  $176 \times 256$  pixels. Relying on Clinical Dementia Rating (CDR) [14], common clinical scale for the staging of dementia, the subjects are comprised of:

- Unchanged CDR = 0: Cognitively healthy population;
- CDR = 0.5: Very mild dementia ( $\sim$  Mild Cognitive Impairment or MCI);
- CDR = 1: Mild dementia.
- CDR = 2: Moderate dementia.

Since our dataset is longitudinal and the same subject’s CDRs may vary (e.g., CDR = 0 to CDR = 0.5), we only use scans with unchanged CDR = 0 to assure certainly healthy scans. As CDRs and MRI scans are not always simultaneously acquired, we label MRI scans with CDRs at the closest date. We only select brain MRI slices including hippocampus/amygdala/ventricles among whole 256 axial slices per scan to avoid over-fitting from AD-irrelevant information; the atrophy of the hippocampus/amygdala/ cerebral cortex, and enlarged ventricles are strongly associated with AD, and thus they mainly affect the AD classification performance of machine learning [15]. Moreover, we discard low-quality MRI slices. The remaining dataset is divided as follows:

- Training set: Unchanged CDR = 0 (408 subjects/1, 133 scans/57, 834 slices);
- Validation set: Unchanged CDR = 0 (55 subjects/155 scans/8, 080 slices),  
CDR = 0.5 (53 subjects/85 scans/4, 607 slices),  
CDR = 1 (29 subjects/45 scans/2, 518 slices),  
CDR = 2 (2 subjects/4 scans/160 slices);
- Test set: Unchanged CDR = 0 (113 subjects/318 scans/16, 198 slices),  
CDR = 0.5 (99 subjects/168 scans/9, 206 slices),  
CDR = 1 (61 subjects/90 scans/5, 014 slices),  
CDR = 2 (4 subjects/6 scans/340 slices).

The same subject’s scans are included in the same dataset. The datasets are strongly biased towards healthy scans similarly to MRI inspection in the clinical routine. During training for reconstruction, we only use the training set containing healthy slices to conduct unsupervised learning.

### 2.2 GAN-based Multiple Adjacent Brain MRI Slice Reconstruction

To model strong consistency in healthy brain anatomy (Fig. 1), in each scan, we reconstruct the next 3 MRI slices from the previous 3 ones using image-to-image GAN (e.g., if a scan includes 40 slices  $s_i$  for  $i = 1, \dots, 40$ , we reconstruct all possible 35 setups:  $(s_i)_{i \in \{1,2,3\}} \mapsto (s_i)_{i \in \{4,5,6\}}$ ;  $(s_i)_{i \in \{2,3,4\}} \mapsto (s_i)_{i \in \{5,6,7\}}$ ;  $\dots$ ;  $(s_i)_{i \in \{35,36,37\}} \mapsto (s_i)_{i \in \{38,39,40\}}$ ). We concatenate adjacent 3 grayscale slices into 3 channels, such as in RGB images. The GAN uses a U-Net-like [16] generator with 4 convolutional layers in encoders and 4 deconvolutional layers in decoders respectively with skip connections as

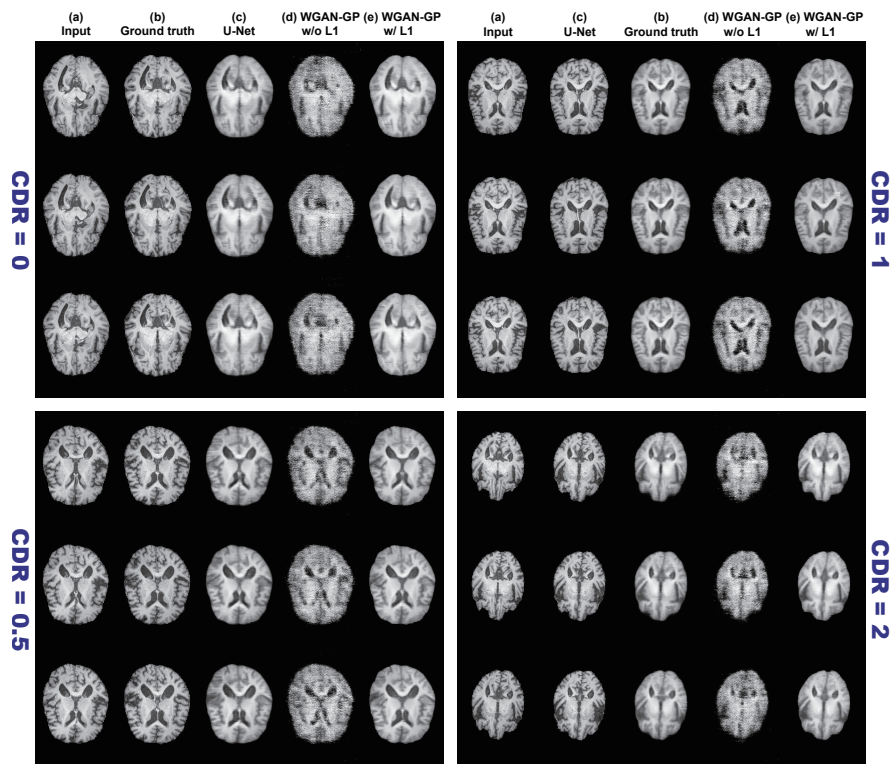


Figure 2: Example brain MRI slices with  $CDR = 0/0.5/1/2$  from test sets: (a) Input 3 real slices; (b) Ground truth next 3 real slices; (c) Next 3 slices reconstructed by U-Net; (d), (e) Next 3 slices reconstructed by WGAN-GP without/with  $\ell_1$  loss.

well as a discriminator with 3 decoders. We apply batch normalization to both convolution with LeakyReLU and deconvolution with ReLU. To confirm how reconstructed images' realism and anatomical continuity affect anomaly detection, we compare the GAN models with different loss functions: (i) Dice loss (i.e., a plain U-Net without the discriminator); (ii) WGAN-GP loss; (iii) WGAN-GP loss +  $100 \ell_1$  loss.

**Implementation Details** Considering its computational speed, U-Net training lasts for 600,000 steps with a batch size of 64 and both GAN trainings last for 300,000 steps with a batch size of 32. We use  $2.0 \times 10^{-4}$  learning rate for Adam optimizer.

### 2.3 Unsupervised Alzheimer's Disease Diagnosis

During validation, we compare the following average/maximum losses per scan (i.e., 8 losses) between reconstructed/ground truth 3 slices (Fig. 1): (i)  $\ell_1$  loss; (ii)  $\ell_2$  loss; (iii) Dice loss; (iv) Structural Similarity loss. For each model's testing, we separately pick the loss showing the highest AUC between  $CDR = 0$  (i.e., healthy population) vs all the other CDRs (i.e., dementia) during validation. As a result, we pick the average  $\ell_2$  loss per scan for all models since squared error is sensitive to outliers and it always outperforms the others. To evaluate its unsupervised AD diagnosis performance for test sets, we show Receiver Operating Characteristics (ROCs)/AUCs between  $CDR = 0$  vs (i) all the other CDRs; (ii)  $CDR = 0.5$ ; (iii)  $CDR = 1$ ; (iv)  $CDR = 2$ . We visualize  $\ell_2$  loss distributions of  $CDR = 0/0.5/1/2$  to know how disease stages affect its discrimination.

## 3 Results

### 3.1 Reconstructed Brain MRI Slices

Fig. 2 illustrates example real MRI slices from test sets and their reconstruction by U-Net and WGAN-GP without/with  $\ell_1$  loss. The WGAN-GP +  $\ell_1$  loss can successfully

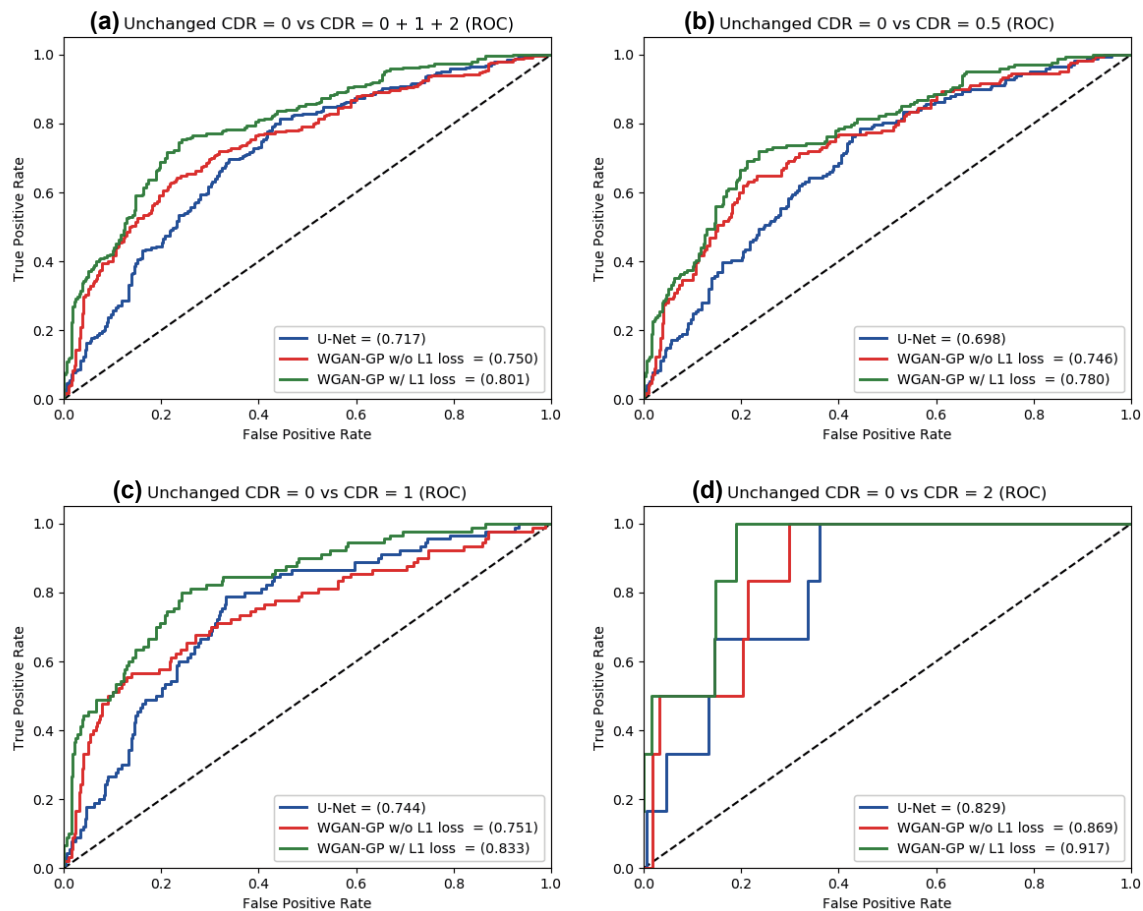


Figure 3: Unsupervised anomaly detection results using average  $\ell_2$  loss per scan on reconstructed brain MRI slices (ROCs and AUCs): unchanged CDR = 0 (i.e., cognitively healthy population) is compared with (a) all the other CDRs (i.e., dementia); (b) CDR = 0.5 (i.e., very mild dementia); (c) CDR = 1 (i.e., mild dementia); (d) CDR = 2 (i.e., moderate dementia).

capture T1w-specific texture and anatomical changes from the previous 3 slices more smoothly than the U-Net and in more detail than the WGAN-GP without  $\ell_1$  loss. Since the models are trained only on healthy slices, reconstructing slices with higher CDRs tends to comparatively fail, especially around hippocampus, amygdala, cerebral cortex, and ventricles due to their insufficient atrophy after reconstruction.

### 3.2 Unsupervised AD Diagnosis Results

Fig. 3 shows ROC curves and their AUCs of unsupervised anomaly detection. Since brains with higher CDRs accompany stronger anatomical atrophy from healthy brains, their AUCs between unchanged CDR = 0 remarkably increase as CDRs increase. Clearly outperforming the other methods in every condition, WGAN-GP +  $\ell_1$  loss achieves excellent AUCs, especially for higher CDRs—it obtains AUC 0.780/0.833/0.917 for CDR = 0 vs CDR = 0.5/1/2, respectively; it derives from  $\ell_1$  loss’ good realism sacrificing diversity (i.e., generalizing well only for unseen images with a similar distribution to training images) and WGAN-GP loss’ ability to capture recognizable structure. Fig. 4 indicates its good discrimination ability even between healthy subjects vs MCI patients (i.e., CDR = 0 vs CDR = 0.5), which is extremely difficult even in a supervised manner [15]. Interestingly, unlike our visual expectation, WGAN-GP without  $\ell_1$  loss outperforms U-Net regardless of its very blurred reconstruction.

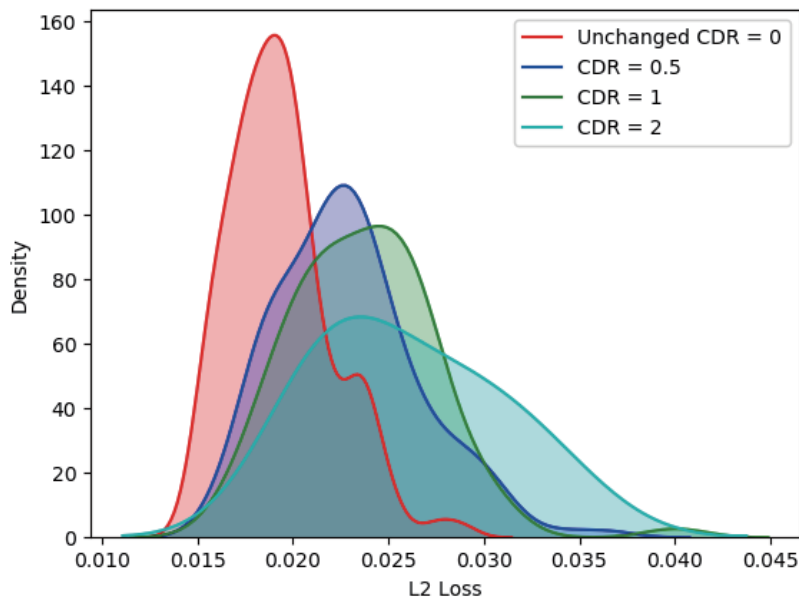


Figure 4: Distributions of average  $\ell_2$  loss per scan evaluated on brain MRI slices with CDR = 0/0.5/1/2 reconstructed by WGAN-GP +  $\ell_1$  loss.

#### 4 Conclusions

Using massive healthy images, our GAN-based multiple MRI slice reconstruction can successfully discriminate AD patients from healthy subjects for the first time in an unsupervised manner; this is thanks to our two-step approach: (*Reconstruction*)  $\ell_1$  loss generalizes well only for unseen images with a similar distribution to training images while WGAN-GP loss captures recognizable structure; (*Diagnosis*)  $\ell_2$  loss clearly discriminates healthy/abnormal data as squared error becomes huge for outliers. Accordingly, this first unsupervised anomaly detection across different disease stages reveals that, like physicians’ way of diagnosis, large-scale healthy data can reliably aid early diagnosis, such as of MCI, while also detecting late-stage disease much more accurately. Since our method well detects the unseen disease hard-to-detect even in supervised learning, this should also discover/alert any anomalies including rare disease, where supervised learning is inapplicable. As future work, we will reconstruct slices from both the previous/next 3 slices (e.g., slices  $s_i$  for  $i = 1, \dots, 9$ ,  $(s_i)_{i \in \{1,2,3,7,8,9\}} \mapsto (s_i)_{i \in \{4,5,6\}}$ ) for robustness. We will investigate more loss functions for both reconstruction/diagnosis. Lastly, we plan to detect/locate various diseases, including rare disease.

#### Acknowledgments

This research was supported by AMED Grant Number JP18lk1010028. Zoltán Ádám Milacski was supported by Grant Number VEKOP-2.2.1-16-2017-00006. The OASIS-3 dataset has Grant Numbers P50 AG05681, P01 AG03991, R01 AG021910, P50 MH071616, U24 RR021382, and R01 MH56584.

#### References

- [1] V. Gulshan, L. Peng, M. Coram et al. “Development and validation of a deep learning algorithm for detection of diabetic retinopathy in retinal fundus photographs”. *JAMA*, vol. 316, no. 22, pp. 2402–2410, 2016.
- [2] C. Han, K. Murao, T. Noguchi et al. “Learning more with less: Conditional PGGAN-based data augmentation for brain metastases detection using highly-rough annotation on MR images”. arXiv preprint arXiv:1902.09856, 2019.
- [3] C. Han, L. Rundo, R. Araki et al. “Combining noise-to-image and image-to-image GANs: Brain MR image augmentation for tumor detection”. arXiv preprint arXiv:1905.13456, 2019.
- [4] C. Han, Y. Kitamura, A. Kudo et al. “Synthesizing diverse lung nodules wherever massively: 3D multi-conditional GAN-based CT image augmentation for object detection”. arXiv preprint

- arXiv:1906.04962, 2019.
- [5] T. Schlegl, P. Seeböck, S. M. Waldstein et al. “Unsupervised anomaly detection with generative adversarial networks to guide marker discovery”. In Proc. International Conference on Information Processing in Medical Imaging (IPMI), pp. 146–157, 2017.
  - [6] M. Freiman, R. Manjeshwar, and L. Goshen. “Unsupervised abnormality detection through Mixed Structure Regularization (MSR) in deep sparse autoencoders”. *Medical Physics*, vol. 46, no. 5, pp. 2223–2231, 2019.
  - [7] H.E. Atlason, A. Love, S. Sigurdsson et al. “Unsupervised brain lesion segmentation from MRI using a convolutional autoencoder”. In Proc. Medical Imaging 2019: Image Processing, pp. 109491H, 2019.
  - [8] C. Baur, B. Wiestler, S. Albarquoni, and N. Navab. “Deep autoencoding models for unsupervised anomaly segmentation in brain MR images”. In Proc. International Conference on Medical Image Computing and Computer-Assisted Intervention (MICCAI) Brainlesion Workshop, pp. 161–169, 2018.
  - [9] D. Zimmerer, S.A. Kohl, J. Petersen et al. “Context-encoding variational autoencoder for unsupervised anomaly detection”. arXiv preprint arXiv:1812.05941, 2018.
  - [10] X. Chen and E. Konukoglu. “Unsupervised detection of lesions in brain MRI using constrained adversarial auto-encoders”. In Proc. International Conference on Medical Imaging with Deep Learning (MIDL), arXiv preprint arXiv:1806.04972, 2018.
  - [11] H. Uzunova, S. Schultz, H. Handels, and J. Ehrhardt. “Unsupervised pathology detection in medical images using conditional variational autoencoders”. *Int. J. Comput. Assist. Radiol. Surg.*, vol. 14, no. 3, pp. 451–461, 2019.
  - [12] I. Gulrajani, F. Ahmed, M. Arjovsky et al. “Improved training of Wasserstein GANs” In Advances in Neural Information Processing Systems (NIPS), pp. 5767–5777, 2017.
  - [13] P.J. LaMontagne, S. Keefe, W. Lauren et al. “OASIS-3: Longitudinal neuroimaging, clinical, and cognitive dataset for normal aging and Alzheimer’s disease”. *Alzheimer’s & Dementia: The Journal of the Alzheimer’s Association*, vol. 14, no. 7, pp. P1097, 2018.
  - [14] J.C. Morris. “The Clinical Dementia Rating (CDR): Current version and scoring rules”. *Neurology*, vol. 43, no. 11, pp. 2412–2414, 1993.
  - [15] C. Ledig, A. Schuh, R. Guerrero et al. “Structural brain imaging in Alzheimer’s disease and mild cognitive impairment: biomarker analysis and shared morphometry database”. *Scientific reports*, vol. 8, no. 1, pp. 11258, 2018.
  - [16] O. Ronneberger, P. Fischer, and T. Brox. “U-Net: Convolutional networks for biomedical image segmentation”. In Proc. International Conference on Medical Image Computing and Computer-Assisted Intervention (MICCAI), pp. 234–241, 2015.